BIOCHEMISTRY
including biophysical chemistry & molecular biology
Article

Biochemistry **2010,** *49,* 10117–10130 10117
DOI: 10.1021/bi1014375

A Comparison of Methanobactins from *Methylosinus trichosporium* OB3b and *Methylocystis* Strain SB2 Predicts Methanobactins Are Synthesized from Diverse Peptide Precursors Modified To Create a Common Core for Binding and Reducing Copper Ions†

Benjamin D. Krentz,‡ Heidi J. Mulheron,‡ Jeremy D. Semrau,§ Alan A. DiSpirito,∥ Nathan L. Bandow,∥ Daniel H. Haft,⊥ Stéphane Vuilleumier,# J. Colin Murrell,@ Marcus T. McEllistrem,‡ Scott C. Hartsel,‡ and Warren H. Gallagher*,‡

‡*Department of Chemistry, University of Wisconsin-Eau Claire, Eau Claire, Wisconsin 54702-4004, United States,* §*Department of Civil and Environmental Engineering, University of Michigan, Ann Arbor, Michigan 48109-2125, United States,* ∥*Department of Biochemistry, Biophysics and Molecular Biology, Iowa State University, Ames, Iowa 50011-3211, United States,* ⊥*J. Craig Venter Institute, 9704 Medical Center Drive, Rockville, Maryland 20850, United States,* #*Université de Strasbourg, UMR 7156 CNRS, 67000 Strasbourg, France, and* @*Department of Biological Sciences, University of Warwick, Coventry CV4 7AL, U.K.*

Received September 6, 2010; Revised Manuscript Received October 17, 2010

ABSTRACT: Methanobactins (mb) are low-molecular mass, copper-binding molecules secreted by most methanotrophic bacteria. These molecules have been identified for a number of methanotrophs, but only the one produced by *Methylosinus trichosporium* OB3b (mb-OB3b) has to date been chemically characterized. Here we report the chemical characterization and copper binding properties of a second methanobactin, which is produced by *Methylocystis* strain SB2 (mb-SB2). mb-SB2 shows some significant similarities to mb-OB3b, including its spectral and metal binding properties, and its ability to bind and reduce Cu(II) to Cu(I). Like mb-OB3b, mb-SB2 contains two five-member heterocyclic rings with associated enethiol groups, which together form the copper ion binding site. mb-SB2 also displays some significant differences compared to mb-OB3b, including the number and types of amino acids used to complete the structure of the molecule, the presence of an imidazolone ring in place of one of the oxazolone rings found in mb-OB3b, and the presence of a sulfate group not found in mb-OB3b. The sulfate is bonded to a threonine-like side chain that is associated with one of the heterocyclic rings and may represent the first example of this type of sulfate group found in a bacterially derived peptide. Acid-catalyzed hydrolysis and decarboxylation of the oxazolone rings found in mb-OB3b and mb-SB2 produce pairs of amino acid residues and suggest that both mb-OB3b and mb-SB2 are derived from peptides. In support of this, the gene for a ribosomally produced peptide precursor for mb-OB3b has been identified in the genome of *M. trichosporium* OB3b. The gene sequence indicates that the oxazolone rings in mb-OB3b are derived from the combination of a cysteine residue and the carbonyl from the preceding residue in the peptide sequence. Taken together, the results suggest methanobactins make up a structurally diverse group of ribosomally produced, peptide-derived molecules, which share a common pair of five-member rings with associated enethiol groups that are able to bind, reduce, and stabilize copper ions in an aqueous environment.

Methanobactins are the first characterized examples of chalkophores, or small, copper-binding peptides, which are involved in the acquisition of copper by methanotrophic bacteria (*1*). Although many methanotrophs produce methanobactins (*2*), the structure of a methanobactin has only been characterized for one produced by *Methylosinus trichosporium* OB3b, a member of the α-Proteobacteria (*3*, *4*). This methanobactin utilizes two oxazolone rings, each associated with an enethiol group, that together create a site for copper ion binding. It also contains seven amino acid residues, along with what appear to be two partial amino acid residues that are associated with each of the oxazolone rings. The chemical structure of mb-OB3b[1] is shown in Figure 1.

Recently, a novel methanotroph, *Methylocystis* strain SB2, has been described (*5*). Like *M. trichosporium* OB3b, it is an α-Proteobacterium that produces a methanobactin. However,

†This work was supported by National Science Foundation Grants CHE 0850701 (B.D.K., H.J.M., S.C.H., and W.H.G.) and CHE-10112271 (A.A.D.), Research Corp. Grant 7638 (S.C.H.), Department of Energy Grants DE-FC26-05NT42431 (J.D.S.) and DE-AC02-05CH11231 (J.C.M. & A.A.D.), NIH Grant 1R01HG004881 (D.H.H.), and the University of Wisconsin-Eau Claire Office of Research and Special Programs (B.D.K., H.J.M., S.C.H., and W.H.G.). The 400 MHz Bruker Avance II NMR spectrometer and the Agilent 6210 ESI-TOF LC−MS instrument used in these studies were funded with National Science Foundation Grants CHE-0521019 and CHE-0619296 to the University of Wisconsin-Eau Claire.

*To whom correspondence should be addressed: Department of Chemistry, University of Wisconsin-Eau Claire, Eau Claire, WI 54702-4004. Telephone: (715) 836-5388. Fax: (715) 836-4979. E-mail: wgallagh@uwec.edu.

[1]Abbreviations: mb-OB3b, methanobactin isolated from *M. trichosporium* OB3b; mb-SB2, methanobactin isolated from *Methylocystis* strain SB2; UV, ultraviolet; DAD, diode array detector; HPLC, high-pressure liquid chromatography; LC−MS, liquid chromatography−mass spectrometry; ESI-TOF, electrospray injection time of flight; NMR, nuclear magnetic resonance; COSY, correlation spectroscopy; TOCSY, total correlation spectroscopy; HSQC, heteronuclear single-quantum coherence spectroscopy; HMBC, heteronuclear multiple-bond coherence spectroscopy; ROESY, rotating frame Overhauser effect spectroscopy; TSP, trimethylsilylpropionate; XPS, X-ray photoelectron spectroscopy; HOPG, highly ordered pyrolytic graphite; RO, reverse osmosis; pMMO, particulate methane monooxygenase; sMMO, soluble methane monooxygenase; Oxa, oxazolone; Imi, imidazolone; MATE, multidrug and toxic compound extrusion; MauG, methylamine utilization G; fwhm, full width at half-maximum.

Published on Web 10/20/2010

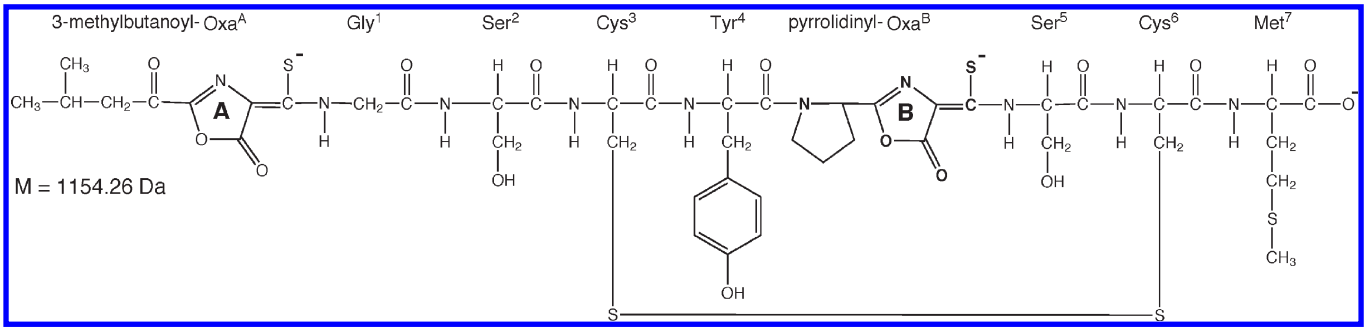

FIGURE 1: Chemical structure of mb-OB3b (*3*). The two oxazolone rings are labeled Oxa^A and Oxa^B.

unlike *M. trichosporium* OB3b, *Methylocystis* strain SB2 can express only the copper- and iron-containing particulate methane monooxygenase (pMMO) (*6*) and not the iron-containing soluble methane monooxygenase (sMMO) (*5*). Furthermore, *Methylocystis* strain SB2 is one of only a handful of methanotrophs shown to be capable of growing on multicarbon substrates, and also of constitutively expressing pMMO, in a manner independent of the growth substrate (*7*). Because *Methylocystis* strain SB2 can express only pMMO, which has an absolute requirement of copper for its activity, the organism is expected to possess a mechanism(s) for acquiring the needed copper from its surroundings.

Here we report the chemical structure for a methanobactin isolated from *Methylocystis* strain SB2 (mb-SB2) and compare it to the previously characterized one produced by *M. trichosporium* OB3b. We find the two molecules share a number of common, core features, specifically, the two heterocyclic ring systems that are each associated with an enethiol and are utilized for copper binding. However, instead of two oxazolone rings, mb-SB2 contains one oxazolone ring and one imidazolone ring. The structures are also similar in that both suggest that they are likely synthesized from peptides made from standard amino acids. We have confirmed this for mb-OB3b by identifying a gene in *M. trichosporium* OB3b that encodes the precursor peptide for mb-OB3b. Besides the difference with the identity of the one heterocyclic ring used for copper binding, mb-SB2 also differs from mb-OB3b in a number of other characteristics. (1) With an exact mass of 851.201 Da, it is ~26% smaller than mb-OB3b. (2) It comprises fewer, and different, amino acid residues than mb-OB3b. (3) It utilizes different residues for the formation of the heterocyclic rings. (4) It contains a sulfate group that is attached to a threonine-like side chain. This may be the first reported finding of an *O*-sulfothreonine in a prokaryotic system. Collectively, the data presented suggest a significant structural diversity among the methanobactins made by methanotrophs. This diversity may be a key factor controlling the structure of methanotrophic communities (*8*).

MATERIALS AND METHODS

Isolation of Methanobactin from Methylocystis Strain SB2 and M. trichosporium OB3b. *Methylocystis* strain SB2 and *M. trichosporium* OB3b were cultured for methanobactin isolation in nitrate mineral medium (*9*) amended with 0.2 μM $CuSO_4$, as previously described (*10*). For ^{15}N-labeled methanobactin, 60% $K^{15}NO_3$ was used as the sole nitrogen source. Methanobactin was separated from cells in the culture medium using a Centramate PE tangential flow filtration system containing an OS030C10 Centramate 30000 Da molecular mass filter cassette (Pall Corp., Framingham, MA). The filtrate was loaded directly onto a 50 mm × 200 mm Dianion HP20 column (Sigma Chemical Co., St. Louis, MO) and washed with 2−3 bed volumes of distilled, deionized H_2O. Methanobactin was eluted with a 60% acetonitrile/40% H_2O mixture, frozen as pellets in liquid nitrogen, and freeze-dried.

UV−Visible Spectrophotometry. UV−visible spectra were recorded on a Cary 50, UV−visible spectrophotometer fitted with a thermostatically controlled sample holder. Spectra were analyzed using *Igor Pro* version 6.1.

HPLC and Mass Spectrometry. Analytical LC−MS runs were conducted on an Agilent 6120 LC−MS instrument equipped with a model 1200 HPLC system and an ESI-TOF mass detector. The mass spectrometer was calibrated using Agilent's ESI-L tuning mix. Samples were loaded on an Agilent 4.6 mm × 150 mm Eclipse XD8-C18 reverse-phase column and eluted at a flow rate of 1 mL/min with a linear gradient from 1 to 99% methanol in H_2O containing either 0.01% acetic acid or 1 mM ammonium acetate. Mass spectra were analyzed using Applied Biosystem's *Analyst*.

Preparative HPLC runs were conducted on a Rainin Dynamax HPLC system equipped with a Varian ProStar 330 UV−visible diode array detector. Runs were analyzed using Varian's *Star Workstation* version 6.3 suite of applications. Samples with concentrations ranging from 4 to 10 mg/mL were loaded on a Hamilton 7 mm × 305 mm PRP-3 semipreparative reverse-phase column and eluted at a flow rate of either 1.5 or 3 mL/min with the same solvents and gradients used for the analytical LC−MS runs.

Accurate Mass Determinations. Accurate mass determinations were achieved via direct injection of a sample into the Agilent 6120 ESI-TOF mass spectrometer. The spectrometer was calibrated in negative ion mode just prior to a run. The samples were also made up to contain internal reference masses. This was done by mixing 5 μL of a 10 mg/mL aqueous solution of methanobactin with 1 mL of the Agilent ESI-L tuning mix. The presence of the internal reference masses allowed us to recalibrate the mass spectrum after the run by using the m/z peaks of two of the mass standards that had m/z values in the same range as our sample, 301.998139 and 601.978977.

Producing Cu-Bound Methanobactin. We made Cu-bound mb-SB2 by dissolving metal-free mb-SB2 to a concentration of approximately 4 mg/mL in 10 mM phosphate buffer (pH 6.5). This solution was taken to a copper:mb molar ratio of 0.5:1 via addition of Cu(II) as aqueous $CuSO_4$. We will show that the copper ion bound to mb-SB2 is Cu(I). One of the reasons for staying below one added Cu(II) per mb-SB2 molecule is to reduce the possibility of contaminating our Cu(I)−mb-SB2 samples with paramagnetic Cu(II) ions, which would affect the ability to conduct NMR studies. As with mb-OB3b, copper binding by

mb-SB2 leads to a release of protons; thus, the pH was readjusted to 6.5 with 100 mM NaOH following the additions of $CuSO_4$.

Cu-bound mb-SB2 [Cu(I)−mb-SB2] was isolated by preparative HPLC as described above. The peak fraction containing Cu(I)−mb-SB2, as judged by it UV−visible spectrum, was collected and pooled with the peak fractions from multiple HPLC runs. The methanol in the pooled fractions was removed prior to lyophilization by either rotary evaporation at 35 °C or dialysis against water using SpectraPor/CE dialysis tubing. Lyophilized samples were stored at −85 °C. This same procedure was also used to prepare an isolated sample of ^{15}N-enriched Cu(I)−mb-SB2.

Because previous studies have indicated no difference in the results obtained when Cu(I)−mb-OB3b is produced either aerobically or anaerobically (*15*), no efforts were made in these studies to exclude oxygen.

NMR Spectroscopy. Nuclear magnetic resonance (NMR) experiments were conducted on a 400 MHz Bruker Avance II NMR spectrometer equipped with a variable-temperature unit and either a 5 mm TXI, Z-gradient indirect detection probe or a 5 mm BBO, Z-gradient broadband probe. Lyophilized mb samples were dissolved to a concentration between 1 and 4 mg/mL in one of three solvents [d_6-DMSO, D_2O, or 90% H_2O/10% D_2O containing 9 mM phosphate (pH 6.5)] and placed in Shigemi NMR tubes (Shigemi, Inc., Allison Park, PA). NMR experiments were conducted at both 5 and 25 °C. Spectra were analyzed using both *Sparky* version 3.115 (University of California, San Francisco, CA) and *iNMR* version 3.5.1 (Nucleomatica, Carabellese, Italy). Spectra were referenced to the HDO peak based on an experimental determination of the position of the HDO peak relative to the TSP peak as a function of temperature.

XPS. X-ray photoelectron spectroscopy (XPS) was performed on a home-built system that includes a model Phoibos-150 hemispherical analyzer (SPECS Surface Nano Analysis, Clearwater, FL). The instrument includes a load lock and operates at a routine base pressure of 2.5×10^{-10} Torr. The spectrometer was calibrated on the $Ag3d_{5/2}$ state for Ar^+-sputtered silver foil and the C1s state from HOPG graphite (Alfa Aesar). Samples were illuminated with Al Kα X-rays ($h\nu$ = 1486.7 eV) from a source operated at 200 W. Spectra for nitrogen, sulfur, and copper were recorded using a consistent spot size of 1.2 mm, normal emission, and a pass energy of 20 eV for all samples. The total illumination time for a sample was ∼45 min. Efforts to evaluate X-ray-induced changes in spectra showed no changes. Using the C1s HOPG signal, a gold foil, and the Cu^{2+} signal from pure $CuCl_2$, we determined that the N1s peak showed no appreciable change in peak shape or binding energy; the peak was consistently observed at 399.6 eV and served as the reference for all spectra collected. No instrumental methods were employed to offset sample charging.

Lyophilized Cu(I)−mb-SB2 was dissolved in a minimal volume of water, dripped onto a HOPG crystal, dried onto the crystal under a stream of N_2, and loaded into the vacuum chamber. We prepared metal-free mb-SB2 samples by dissolving the methanobactin in a minimal amount of water and deposited on the HOPG crystal in the same manner as the Cu(I)−mb-SB2 sample. No efforts were made to handle solutions in an anaerobic environment.

Spectra were fitted to a Shirley background, with peaks having a fixed 30:70 Gaussian:Lorentzian ratio using the XPS fitting program CASA XPS. The S2p peak splitting was not resolved but fit to two states. The $2p_{1/2}$ area was constrained to be half that of $2p_{3/2}$ and shifted to a higher binding energy by 1.18 eV. All states were constrained to a fwhm between 1.9 and 2.2 eV, based on the fwhm of 1.9 eV observed for the N1s peak.

Acid-Catalyzed Hydrolysis of Metal-Free mb-OB3b and mb-SB2. We conducted acid-catalyzed hydrolysis of metal-free mb-OB3b and mb-SB2 by dissolving lyophilized methanobactin in either aqueous acetic acid or HCl. The acetic acid concentrations ranged from 0.01% (1.7 mM) to 0.1% (17 mM), while the HCl concentrations ranged from 1 mM to 1 M. To monitor hydrolysis using UV−visible spectrophotometry, 50 μM mb was prepared and the reaction monitored in a sealed cuvette at 25 °C in a thermostatically controlled sample holder. In other experiments, the products of hydrolysis were isolated and characterized. For these experiments, the mb concentrations ranged from 4 to 10 mg/mL in either acid and the mixtures were incubated in the dark at room temperature. The hydrolysis was halted by neutralization with either NaOH or NH_4OH prior to fractionation of the products by preparative HPLC.

Genomics Analyses. All nucleotide sequences available from NCBI for *M. trichosporium* OB3b were collected and searched by tblastn (*11*) with the sequence LXGSCYPXSCM. The maximum possible start-to-stop open reading frame containing the matching sequence, found in GenBank sequence ADVE01000073.1 but not annotated as a gene, was translated to protein and searched (with translation) by tblastn against NCBI's nonredundant nucleic acid database, with an *E* value limit set to 100 and low-complexity filtering turned off. For the single matching sequence found, the maximal possible start-to-stop open reading was identified, translated to protein, and aligned with *MUSCLE* (*12*) with the *M. trichosporium* OB3b sequence.

To identify a candidate maturation enzyme cluster for methanobactin precursor sequences, we searched proteins encoded near the putative methanobactin precursor sequence from ADVE01000073.1 against the NCBI nonredundant protein sequence database with default parameters.

Solvents and Reagents. All solvents and reagents used were reagent grade or better. We further purified house RO water by passing it through a Barnstead NANOpure II system to produce water with a resistivity of > 17 MΩ cm.

RESULTS

Comparison of UV−Visible Absorption by mb-SB2 and mb-OB3b and Its Response to Cu(II) Exposure. The UV−visible spectrum of mb-SB2, though not identical to that of mb-OB3b, shares many of the same features (Figure 2). In particular, at wavelengths above 310 nm there are two characteristic peaks. For metal-free mb-OB3b, these are located at 394 and 340 nm and have previously been assigned to the chromophoric A and B oxazolone ring systems, respectively (Figure 1) (*3*). The spectrum for metal-free mb-SB2 shows a similar pair of peaks at 387 and 338 nm. The spectral changes for mb-SB2 accompanying the exposure to Cu(II) are also similar to those observed with mb-OB3b (*13*). We will show below that like the case for mb-OB3b, the copper that is found bound to mb-SB2 is reduced to Cu(I). Though the spectral changes that occur with each addition of Cu(II) are complete in less than a second, 5 min was allowed to elapse between each addition and the acquisition of the corresponding spectrum. The changes in the UV−visible spectrum upon exposure to Cu(II) suggest that like mb-OB3b, mb-SB2 contains a pair of chromophoric groups that are involved in Cu ion binding.

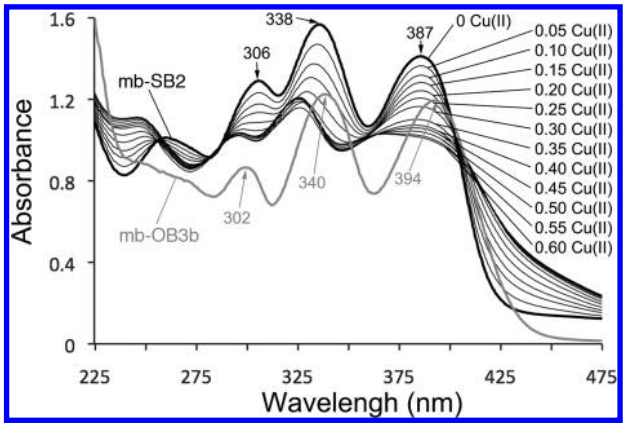

FIGURE 2: UV−visible absorption spectra of mb-SB2 as isolated (black trace) and following additions of $CuSO_4$. The labeled trace for metal-free mb-OB3b is included for comparison. The labels on the right give the molar ratio of Cu(II) added per mb-SB2.

Mass Spectrometry of Metal-Free mb-SB2 Reveals a Substantially Different Mass Compared to mb-OB3b. An accurate mass determination was made on the metal-free mb-SB2. Figure S1 (Supporting Information) shows the *m*/*z* peaks obtained for the −2 charged species of metal-free mb-SB2, $[M - 2H^+]^{2-}$. We also observed the $[M - H^+]^{1-}$ and $[M - 3H^+]^{3-}$ charged species (data not shown), along with *m*/*z* peaks for mb-SB2 in complexes with ions from adventitious sources, specifically, the −2 charged species of mb-SB2 in a complex with one sodium ion, $[M + Na^+ - 3H^+]^{2-}$, one potassium ion, $[M + K^+ - 3H^+]^{2-}$, and one zinc ion, $[M + Zn^{2+} - 4H^+]^{2-}$. On the basis of these six species, the exact mass (±standard error) for the neutral, metal-free mb-SB2 was determined to be 851.2006 ± 0.0012 Da. This mass is 26% lower than for the neutral form of metal-free mb-OB3b (1154.2636 Da) (*3*) and indicates some marked differences in composition between the two methanobactins.

Mass Spectrometry of Cu-Bound mb-SB2 Reveals That a Single Cu Ion Is Bound as Cu(I). Cu-bound mb-SB2 was prepared as described in Materials and Methods and isolated by preparative HPLC. Before being isolated, the sample was first characterized by LC−MS. Figure 3 shows an example of an elution profile for unpurified Cu-bound mb-SB2, along with the mass spectrum for the largest peak fraction. This peak contains both the −1 and −2 charged species of a single component. The isotope pattern (inset of Figure 3) is that expected for a Cu-bound peptide. The calculated mass for the neutral, metal-free mb-SB2, based on the *m*/*z* values for two observed Cu-bound species, is 851.201 Da, when the species are assumed to be $[M + Cu^+ - 2H^+]^{1-}$ and $[M + Cu^+ - 3H^+]^{2-}$. This is in good agreement with the mass determined directly from the metal-free form of mb-SB2 (851.2006 Da). It is significant to note that the mass of the Cu-bound mb-SB2 supports an assertion that the bound copper ion is Cu(I), because the binding of a Cu(II) ion ($[M + Cu^{2+} - 3H^+]^{1-}$ and $[M + Cu^{2+} - 4H^+]^{2-}$) would result in a calculated neutral mass that is 1 Da lower. Later we will show that this assertion is supported by XPS measurements. Like mb-OB3b, mb-SB2 is able to reduce the Cu(II) ion to Cu(I) upon binding and to do so without altering the chemical structure of the mb-SB2 that binds the Cu(I) ion. The binding of copper ions by mb-OB3b is known to dramatically increase its chemical stability (*14*, *15*). We have found the same to be true for Cu(I)−mb-SB2. Consequently, we chose to conduct further structural analyses of Cu(I)−mb-SB2.

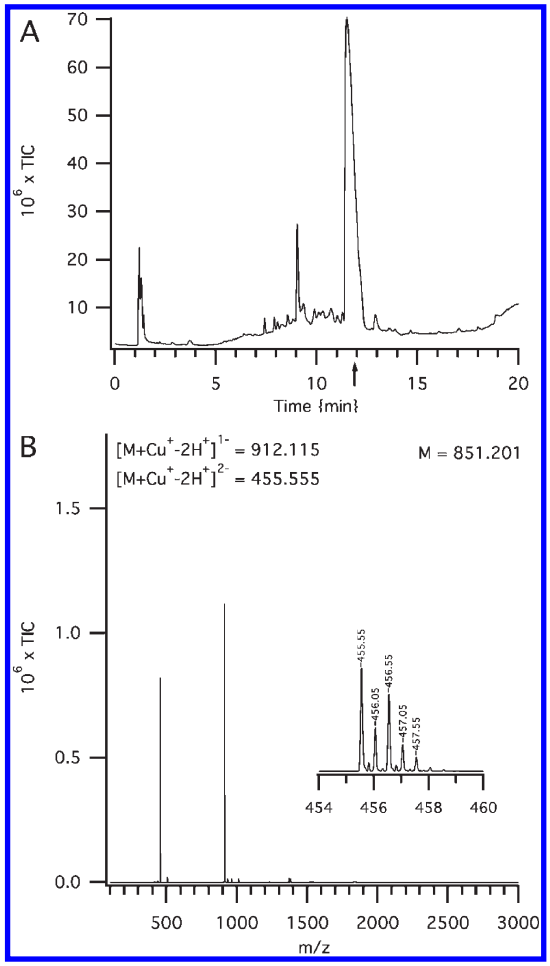

FIGURE 3: (A) LC−MS elution profile for Cu(I)−mb-SB2 after exposure to 0.5 Cu(II) per mb-SB2. (B) Mass spectrum of the peak fraction, which is indicated by the arrow in panel A. The inset shows the isotope pattern for the peak at *m*/*z* 455.555.

Chemical Structure of Cu(I)−mb-SB2 As Determined by NMR Spectroscopy. Figure 4 shows the ^1H and ^{15}N spectra of Cu(I)−mb-SB2. The narrow lines in the ^1H spectrum support the argument that the bound copper is Cu(I), and not paramagnetic Cu(II). The ^{15}N spectrum reveals that mb-SB2 contains 11 nitrogen atoms, one more than mb-OB3b. A variety of two-dimensional (2D) experiments were conducted on Cu(I)−mb-SB2 to make resonance assignments and to observe the $^1H-^1H$, $^1H-^{13}C$, and $^1H-^{15}N$ correlations that were used to deduce a chemical structure for mb-SB2. These experiments included $^1H-^1H$ COSY, $^1H-^1H$ TOCSY, $^1H-^1H$ ROESY, $^1H-^{13}C$ HSQC, $^1H-^{13}C$ HMBC, $^1H-^{15}N$ HSQC, and $^1H-^{15}N$ HMBC. The ^1H, ^{13}C, and ^{15}N resonance assignments for mb-SB2 are listed in Table S1 (Supporting Information), and a summary of the observed correlations is shown in Figure S2 (Supporting Information). Figure 5 shows the proposed structure of mb-SB2 based on the NMR analyses. This structure highlights a number of substantial differences compared to the mb-OB3b structure. The A-ring is an imidazolone instead of an oxazolone. In support of this finding, the N^1 atom of the A-ring, along with the attached H^1 atom, is observed in both direct and indirect detection experiments. In the ^1H spectrum (Figure 4A), the H^1 atom appears as a singlet, downfield at 11.26 ppm, and in the ^{15}N spectrum (Figure 4B), the N^1 atom is located at 174 ppm, between the amide nitrogens (111−145 ppm) and the two remaining ring nitrogens, N^3 (232 and 292 ppm). The assignment of the 292 ppm resonance to the N^3 atom of the imidazolone A-ring was

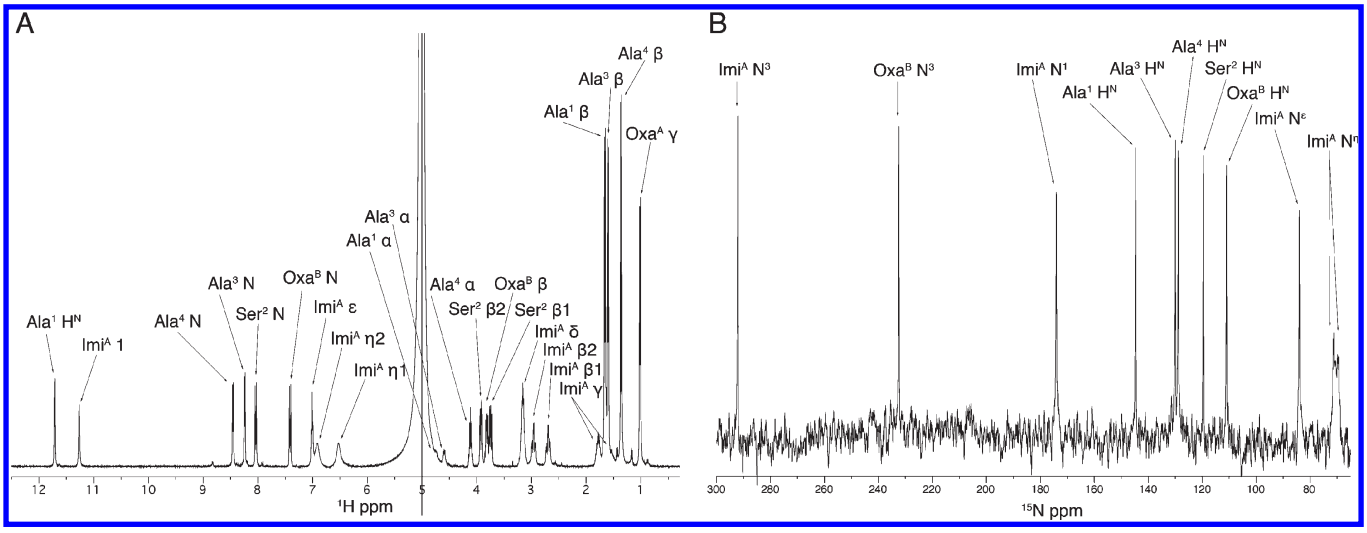

FIGURE 4: (A) ^{1}H spectrum of Cu(I)−mb-SB2 in a 90% H_2O/10% D_2O mixture at 5 °C. (B) ^{15}N spectrum of ^{15}N-enriched Cu(I)−mb-SB2 in a 90% H_2O/10% D_2O mixture at 5 °C.

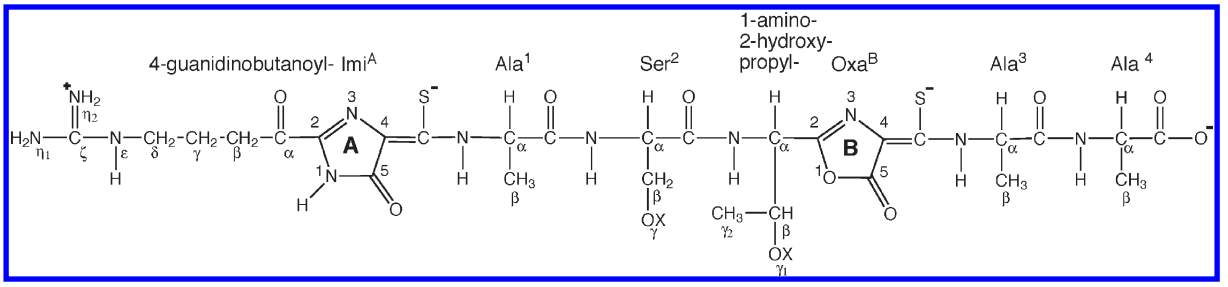

FIGURE 5: Proposed primary structure for mb-SB2 based on the NMR analyses. The correlations observed in the 2D correlation experiments that led to this structure can be found in Figure S2 of the Supporting Information. The A-ring imidazolone is labeled as Imi^{A}, while the B-ring oxazolone is labeled as Oxa^{B}. On the basis of mass, this is not the complete structure.

made on the basis of multibond correlations observed in the ^{1}H−^{15}N HMBC experiment (Figure S2 of the Supporting Information). Like mb-OB3b, both rings are associated with what looks like a portion of an amino acid, but the identities of these amino acids differ in all four cases observed so far. The carbonyl carbons from the partial amino acids appear to be incorporated as the C^{2} atom of the adjacent ring. Also, for the partial amino acids that are associated with the A-rings, it appears that the C$^{\alpha}$ atom is deaminated and oxidized to a ketone. For mb-OB3b, the partial amino acid associated with the A-ring is leucine while that with the B-ring is proline (Figure 1). For mb-SB2, the partial amino acid associated with the A-ring is arginine while that with the B-ring is threonine (Figure 5). The identities of the intact amino acid residues are also quite different. For mb-OB3b, they include Gly^{1}, Ser^{2}, Cys^{3}, Tyr^{4}, Ser^{5}, Cys^{6}, and Met^{7}, while for mb-SB2, they include Ala^{1}, Ser^{2}, Ala^{3}, and Ala^{4}. The only unusual feature found in the NMR spin systems for the amino acids in mb-SB2 was the notable downfield shift for the amide proton of the Ala^{1} residue, at 11.7 ppm (Figure 4A). The resonance for the corresponding amide nitrogen of Ala^{1}, at 145 ppm, is also the furthest downfield of all of the amide nitrogens (Figure 4B). The unusual downfield shift in the amide proton for Ala^{1} was observed for both the Cu(I) and metal-free form of mb-SB2, suggesting the downfield shift is due to the participation of the amide nitrogen in the extended conjugated system that is set up by the adjacent imidazolone. In mb-OB3b, the amide proton for the Gly^{1} residue (Figure 1), which occupies the equivalent position adjacent to the A-ring oxazolone, is also shifted the furthest downfield for mb-OB3b, but only to 9.28 ppm (*3*).

The structure shown in Figure 5 is not, however, a complete structure. The calculated exact mass for this structure is 771.243 Da, which is 79.957 Da lighter than the experimentally determined mass for mb-SB2 (851.2006 Da). This difference immediately suggests two possibilities, a phosphonate group (-HPO_3^-) or a sulfonate group (-SO_3^-), each of which has a mass of 79.967 or 79.957 Da, respectively. A phosphonate group was ruled out on the basis of a ^{31}P NMR experiment (data not shown), which demonstrated that mb-SB2 contains no phosphorus atoms. To corroborate the presence of a sulfonate group, we turned to X-ray photoelectron spectroscopy (XPS).

X-ray Photoelectron Spectroscopy Confirms That mb-SB2 Contains a Sulfate Group and a Cu(I) Ion in Its Cu-Bound Form. XPS can identify elements in a sample based on the kinetic energy of the core electrons that are ejected from a sample upon X-ray irradiation. It is also sensitive to the oxidation state of an element. XPS spectra were recorded for both metal-free and Cu(I)-bound mb-SB2. The Cu2p$_{3/2}$ peak for Cu(I)−mb-SB2 shows a single peak with a fwhm of 1.91 eV (data not shown). The fwhm is in agreement with that observed for the N1s peak and indicates a single state for the copper in Cu(I)−mb-SB2. The binding energy for the Cu2p$_{3/2}$ electron was found to be 931.9 eV, in close agreement with the Cu2p$_{3/2}$ peak reported for Cu(I) chloride (932.5 eV) (*16*) but not for Cu(II) chloride (935 eV). This provides additional evidence that Cu-bound mb-SB2 contains a Cu(I) ion.

Figure 6 shows the region of the XPS spectrum for the S2p electrons. Two distinct peaks are observed for both the metal-free and Cu(I)-bound mb-SB2 samples. For the metal-free mb-SB2,

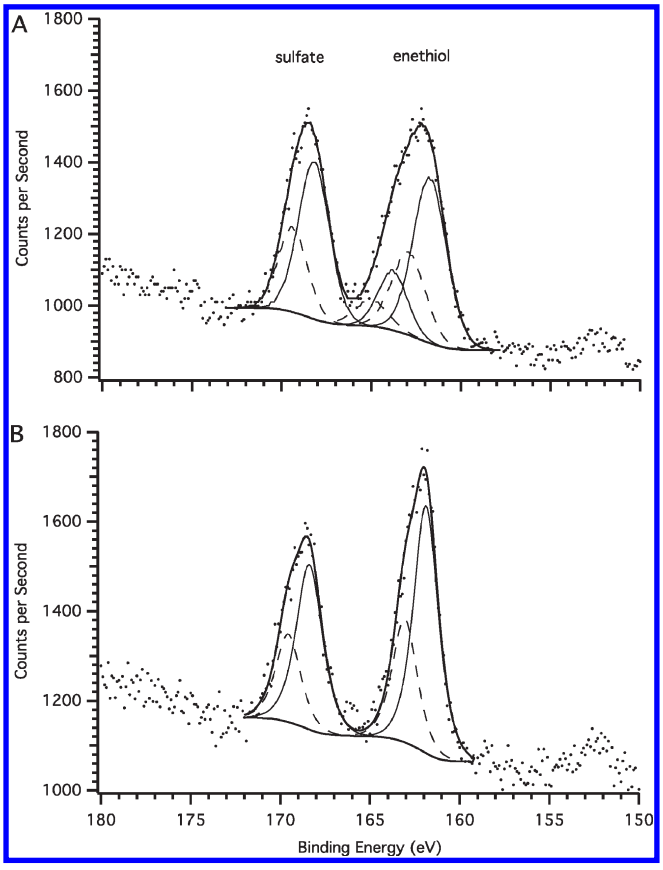

FIGURE 6: XPS spectra for (A) metal-free mb-SB2 and (B) Cu(I)−mb-SB2. The states were fit to pairs of peaks to account for spin−orbital splitting; the solid fit curves are for the $S2p_{3/2}$ electrons, while the dashed fit curves are for the $S2p_{1/2}$ electrons.

the $S2p_{3/2}$ peak with the higher binding energy is found at 169.4 eV, while for Cu(I)−mb-SB2, it is found at 169.5 eV. Both fit well to a peak with a fwhm in the range of 1.9−2.2 eV, indicating a single state for this sulfur. On the basis of the data reported for various sulfate compounds in the NIST XPS database (*16*), a sulfur peak with a binding energy in this range is consistent with a highly oxidized sulfur, such as a sulfate (167.9−168.7 eV). We therefore assign this peak to a sulfate.

The sulfur peak with the lower binding energy located at 161.9 eV for Cu(I)−mb-SB2 can also be fit to a peak with a fwhm in the range of 1.9−2.2 eV (Figure 6B). This binding energy is consistent with a more highly reduced state for sulfur, such as thiols, disulfides, and thioamides, which have values reported in the NIST tables that range from 162.1 to 164.1 eV (*16*). Consequently, we are assigning this peak to the two enethiols found in mb-SB2. For the metal-free mb-SB2 (Figure 6A), the fit residuals indicate that this peak cannot be reasonably fit to a single state with a fwhm in the range of 1.9−2.2 eV. This indicates that for metal-free mb-SB2, the enethiols experience multiple environments. We therefore fit this peak to two states. The lower-energy state is positioned at 161.7 eV, while the higher-energy state is positioned at 163.8 eV. The binding of Cu(I) by mb-SB2 coalesces these two states into a single state (Figure 6B). A similar coalescence upon copper binding has also been observed for mb-OB3b (*13*) and suggests that the enethiol sulfurs in mb-SB2 are directly involved in Cu(I) binding, as they are for mb-OB3b (*4*).

Given two enethiol sulfurs along with a single sulfate sulfur, the ratio of the areas for the enethiol peak to the sulfate peak is expected to be 2:1; however, the observed ratio for the peak areas, for both metal-free and Cu-bound mb-SB2, is only 1.4:1. Because the intensity of an XPS signal is quite sensitive to the depth from the surface that an atom finds itself in the dried sample, a possible explanation for this discrepancy could be that the highly charged sulfate positions itself closer to the surface as the mb-SB2 is dried down onto the HOPG crystal. On the basis of the two-state fit for the enethiol peak in the metal-free mb-SB2 (Figure 6A), it appears this causes one of the two enethiols to be pushed farther from the surface.

Chemically, the most likely location in mb-SB2 for a sulfate group, which is also compatible with the NMR-determined structure, is either O-sulfonation of the serine side chain or the threonine-like side chain (designated by X's in Figure 5). Below we provide evidence of the latter. When the sulfate is included, the calculated exact mass for mb-SB2 is 851.1997 Da, which now agrees within 1 ppm with the experimentally determined mass of 851.2006 Da.

Acid-Catalyzed Hydrolysis of the Oxazolone Rings in Both mb-OB3b and mb-SB2 Suggests a Peptide Origin for mb-OB3b and mb-SB2 and Helps to Locate the Sulfate Group in mb-SB2. A comparison of the acid-catalyzed hydrolysis of mb-OB3b and mb-SB2 reveals some interesting structural features for methanobactins and helps to explain the observed fragility of metal-free methanobactins (*14*, *15*). The lactone groups of the oxazolone rings in mb-OB3b have previously been shown to be susceptible to methanolysis (*3*). We have also observed that the oxazolones in metal-free methanobactins are susceptible to acid-catalyzed hydrolysis. This is shown in Figure 7A, where the complete loss of the B-ring in mb-OB3b, as indicated by the loss of absorbance at 340 nm, occurs in slightly more than 1 day upon exposure to 1 mM HCl. A similar result is obtained with 0.01% (1.7 mM) acetic acid (data not shown). Panels B and C of Figure 7 show the results obtained for acid-catalyzed hydrolysis in 10 and 100 mM HCl, respectively, and indicate that increasing the concentration of HCl to 100 mM leads to the loss of both oxazolone rings in 2.5 days (Figure 7C), as indicated by the loss of UV−visible absorption at both 340 and 394 nm.

The products obtained after hydrolysis of metal-free mb-OB3b with 100 mM HCl for 15 h were further characterized after isolation by preparative HPLC. When preparative HPLC was conducted as described in Materials and Methods, five peak fractions were observed. None contained intact mb-OB3b as judged by mass spectrometry, while two contained species characteristic of mb-OB3b that had lost either one or both of its oxazolone rings. The UV−visible and mass spectra for these two fractions are shown in Figure 8 (A−D). The primary component in fraction 1 has an ion at m/z 563.13 for a species with a −2 charge (Figure 8B). Assuming it is the $[M - 2H^+]^{2-}$ species, this corresponds to a neutral mass of 1128.28 Da. This is 25.98 Da less than the mass of the neutral metal-free mb-OB3b (1154.26 Da). For simple hydrolysis of an oxazolone ring, the mass is expected to increase by 18.01 Da ($+H_2O$). The observed decrease indicates a loss of 43.99 Da following hydrolysis and suggests the α-carboxylic acid group formed by hydrolysis of the oxazolone ring is lost as CO_2. Scheme 1B shows a proposed structure for metal-free mb-OB3b after hydrolysis and decarboxylation of the B-ring, which has a calculated neutral mass that agrees with what is observed (1128.28 Da). The formation of a glycine residue as a consequence of the decarboxylation has been confirmed by NMR spectroscopy (data not shown).

Similarly, the primary component found in fraction 2 (Figure 8D) is consistent with a mb-OB3b molecule that has lost both its oxazolone rings through hydrolysis and decarboxylation.

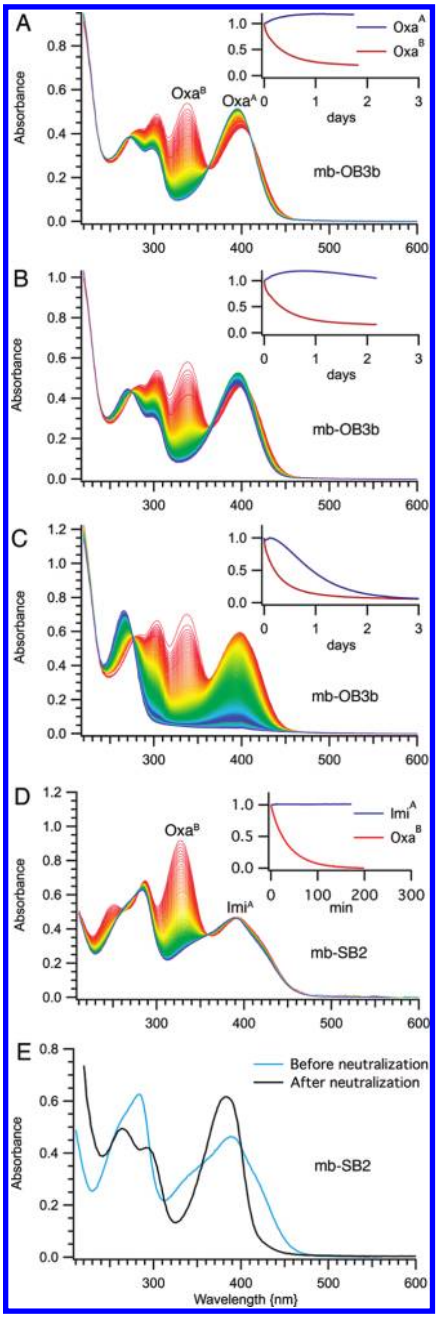

FIGURE 7: (A−C) UV−visible monitoring of the hydrolysis of the oxazolone rings in metal-free mb-OB3b at 25 °C. The experiments were conducted in (A) 1, (B) 10, and (C) 100 mM HCl. (D) UV−visible monitoring of the hydrolysis of the oxazolone ring in metal-free mb-SB2 in 0.1% (17 mM) acetic acid at 25 °C. (E) Effect of neutralization on the UV−visible spectrum of mb-SB2 after hydrolysis in 0.1% acetic acid for 200 min. For panels A−D, the overlaid spectra progress from red (initial time point) to blue (final time point). For panels A−C, the peak at 340 nm corresponds to the oxazolone B-ring in mb-OB3b while that at 394 nm corresponds to the oxazolone A-ring. For panels D and E, the peak at 338 nm corresponds to the oxazolone B-ring in mb-SB2 while that at 389 nm corresponds to the imidazolone A-ring. The insets in panels A−D follow the kinetics in the absorbance changes for the two rings.

The UV−visible spectrum for this species shows a single peak at 267 nm and agrees well with that reported for thioamide-containing peptides (*17*). The ion at *m*/*z* 550.14 observed for the −2 charged species gives a neutral mass of 1102.30 Da, which agrees with the calculated neutral mass for the structure proposed in Scheme 1C. The hydrolysis and decarboxylation of both oxazolone rings in mb-OB3b convert mb-OB3b into an 11-residue peptide that is modified to contain two thioamide-containing residues (Gly^A-Ψ and Gly^B-Ψ) and an N-terminal leucine residue with its C^α atom deaminated and oxidized to a ketone (Scheme 1C).

Similar hydrolysis experiments were conducted with metal-free mb-SB2. Figure 7D shows the results obtained when mb-SB2 is exposed to 0.1% acetic acid (17 mM) at 25 °C. The oxazolone (B-ring) in mb-SB2 appears to be even more susceptible to hydrolysis than the corresponding ring in mb-OB3b, as the hydrolysis appears complete after only 200 min, compared to 2 days for mb-OB3b when the hydrolysis was conducted in 10 mM HCl. The imidazolone (A-ring), on the other hand, appears to be quite resistant to hydrolysis; we have found that overnight exposure to HCl at concentrations as high as 1 M does not lead to a loss of this ring (data not shown). This stability supports the finding that the A-ring in mb-SB2 is not an oxazolone.

The lower pH that exists during hydrolysis causes a number of changes in the UV−visible spectrum for mb-SB2. Figure 7E shows the effect that neutralization has on the UV−visible spectrum of the sample after hydrolysis. This spectrum looks quite similar to that obtained for mb-OB3b after hydrolysis and decarboxylation of its oxazolone B-ring (compare to Figure 8A).

To further characterize the products of hydrolysis of mb-SB2, a sample of mb-SB2 was subjected to hydrolysis in 10 mM HCl at room temperature for 7 days. Subsequent LC−MS analysis revealed a single major peak fraction. Figure 8E shows the UV−visible and mass spectra for the material in the major peak fraction. The mass spectrum (Figure 8F) indicates the fraction contains both the −1 and −2 charged species of a single component with a neutral mass of 825.22 Da. This agrees with that expected after hydrolysis and decarboxylation of the oxazolone ring in mb-SB2. The UV−visible spectrum for the hydrolyzed mb-SB2 is nearly identical to that observed for mb-OB3b after hydrolysis of its B-ring oxazolone (compare panel E of Figure 8 to panel A).

The major peak fraction for mb-SB2 after exposure for 7 days to 10 mM HCl was isolated by preparative HPLC and analyzed by NMR spectroscopy. The analyses were conducted in both D_2O and a 90% H_2O/10% D_2O mixture at 5 °C. For comparison, a similar analysis was conducted on intact metal-free mb-SB2 in D_2O at 5 °C. A number of NMR experiments were conducted, including $^1H-^1H$ TOCSY, $^1H-^{13}C$ HSQC, and $^1H-^{13}C$ HMBC. The resonance assignments for the hydrolyzed mb-SB2 and intact metal-free mb-SB2 are listed in Table S2 (Supporting Information). Figure 9 shows an overlay of the $^1H-^{13}C$ HSQC spectra for the hydrolyzed and intact mb-SB2 in D_2O. The largest chemical shifts occur in the region of the B-ring oxazolone, which is converted to a threonine residue with a glycine residue upon hydrolysis and decarboxylation. The C^α atom for the newly formed glycine, which is derived from the C^4 atom of the oxazolone ring, can be clearly seen by the pair of $^1H-^{13}C$ cross-peaks in the $^1H-^{13}C$ HSQC spectrum (Figure 9). The Oxa^B $H^\alpha-C^\alpha$ cross-peak, which becomes the Thr^B $H^\alpha-C^\alpha$ cross-peak after hydrolysis, shows the largest shift, and the Ala^3 $H^\alpha-C^\alpha$ resonance, arising from the Ala^3 residue adjacent to the B-ring oxazolone, also shows a noticeable shift.

As mentioned earlier, the most likely location for the sulfonate group that is consistent with our NMR analyses of mb-SB2 is the O^γ atom of either the serine side chain or the threonine-like side chain associated with the B-ring oxazolone (designated by X's in Figure 5). We have shown that with the loss of the B-ring oxazolone, the threonine-like side chain is converted to a true

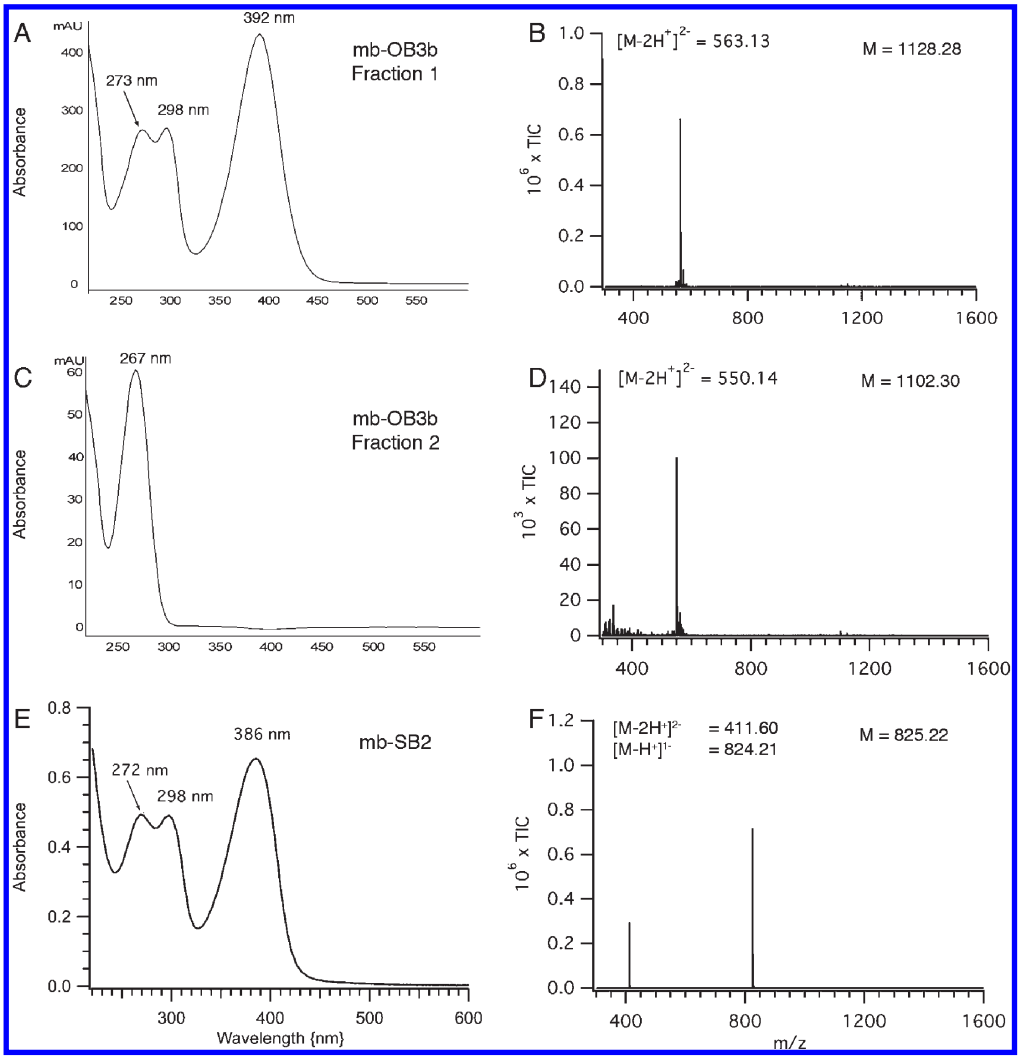

FIGURE 8: (A and C) UV−visible spectra for two of the fractions obtained after exposure of mb-OB3b to 100 mM HCl for 15 h at 25 °C and (B and D) corresponding mass spectra for the same two fractions. (E) UV−visible spectrum for the major fraction obtained after exposure of mb-SB2 to 10 mM HCl for 7 days at 25 °C and (F) corresponding mass spectrum.

threonine. The ^{1}H assignments for the H$^{\beta}$ protons of the serine and the threonine after the loss of the B-ring oxazolone provide evidence that the sulfonate group is attached to the threonine side chain and not the serine side chain (Table S2 of the Supporting Information). The assignment for the two H$^{\beta}$ protons of the Ser^{2} side chain is 3.91 ppm, while that for the single H$^{\beta}$ proton of the Thr^{B} residue is 4.89 ppm. Jaeger et al. (*18*) have determined ^{1}H assignments for hexapeptides in D_2O, which they synthesized to contain either an O-*sulfo*-serine or an O-*sulfo*-threonine. They looked at two different examples for each. For serine, the chemical shift of the H$^{\beta}$ protons moves downfield from 3.91 to 4.39 ppm upon sulfonation of ARGASG to ARGAS(SO_3H)G and from 3.96 to 4.41 ppm upon sulfonation of ARGDSG to ARGDS(SO_3H)G. For threonine, the chemical shift for the H$^{\beta}$ proton moves downfield from 4.39 to 4.87 ppm upon sulfonation of ARGATG to ARGAT(SO_3H)G and from 4.37 to 4.90 ppm upon sulfonation of ARGDTG to ARGDT(SO_3H)G. In light of the findings of Jaeger et al., our assignments of 3.91 ppm for the Ser^{2} H$^{\beta}$ atom and 4.89 ppm for the Thr^{B} H$^{\beta}$ atom indicate that the threonine-like side chain of intact mb-SB2 is the site of sulfonation, and not the serine.

As part of our NMR analysis of the hydrolyzed mb-SB2, we also conducted ^{1}H−^{13}C HMBC experiments that gave us a set of inter-residue correlations that further support our proposed structure for the intact and hydrolyzed mb-SB2 molecule. These data are summarized in Figure S3 of the Supporting Information. Scheme 2A shows our proposed structure for the complete, intact mb-SB2 molecule, which is supported now by ^{1}H, ^{13}C, and ^{15}N NMR spectroscopy, mass spectrometry, XPS, and chemical hydrolysis data. Scheme 2B shows the product obtained after hydrolysis of the B-ring oxazolone.

Genomic Analysis of the Genome for M. trichosporium OB3b Identifies a Gene for the mb-OB3b Precursor Peptide. The hydrolysis results for both metal-free mb-OB3b and mb-SB2 suggest that these methanobactins are derived from peptides. Given the availability of a partially sequenced genome for *M. trichosporium* OB3b, a search was done to see if a gene for a precursor peptide for mb-OB3b could be located. A BLAST search with on-the-fly translation of all available nucleotide sequences from *M. trichosporium* OB3b was performed with the peptide sequence LXGSCYPXSCM, derived from the chemical structure of the hydrolyzed mb-OB3b (Scheme 1C). The X's indicate the locations of the unknown resides that reside where the glycine residues are found in hydrolyzed mb-OB3b. A matching region was found in which both unknown X residues were found to be cysteine. The maximum possible open reading frame is eeaMTVKIAQKKVLPVIGRAAA**LCGSCYPCSCM**, where residues shown as lowercase letters lie upstream of the first

Scheme 1: Primary Structure of mb-OB3b after Hydrolysis and Decarboxylation of the B-Ring Oxazolone (A to B) and Hydrolysis and Decarboxylation of Both Oxazolones (B to C)[a]

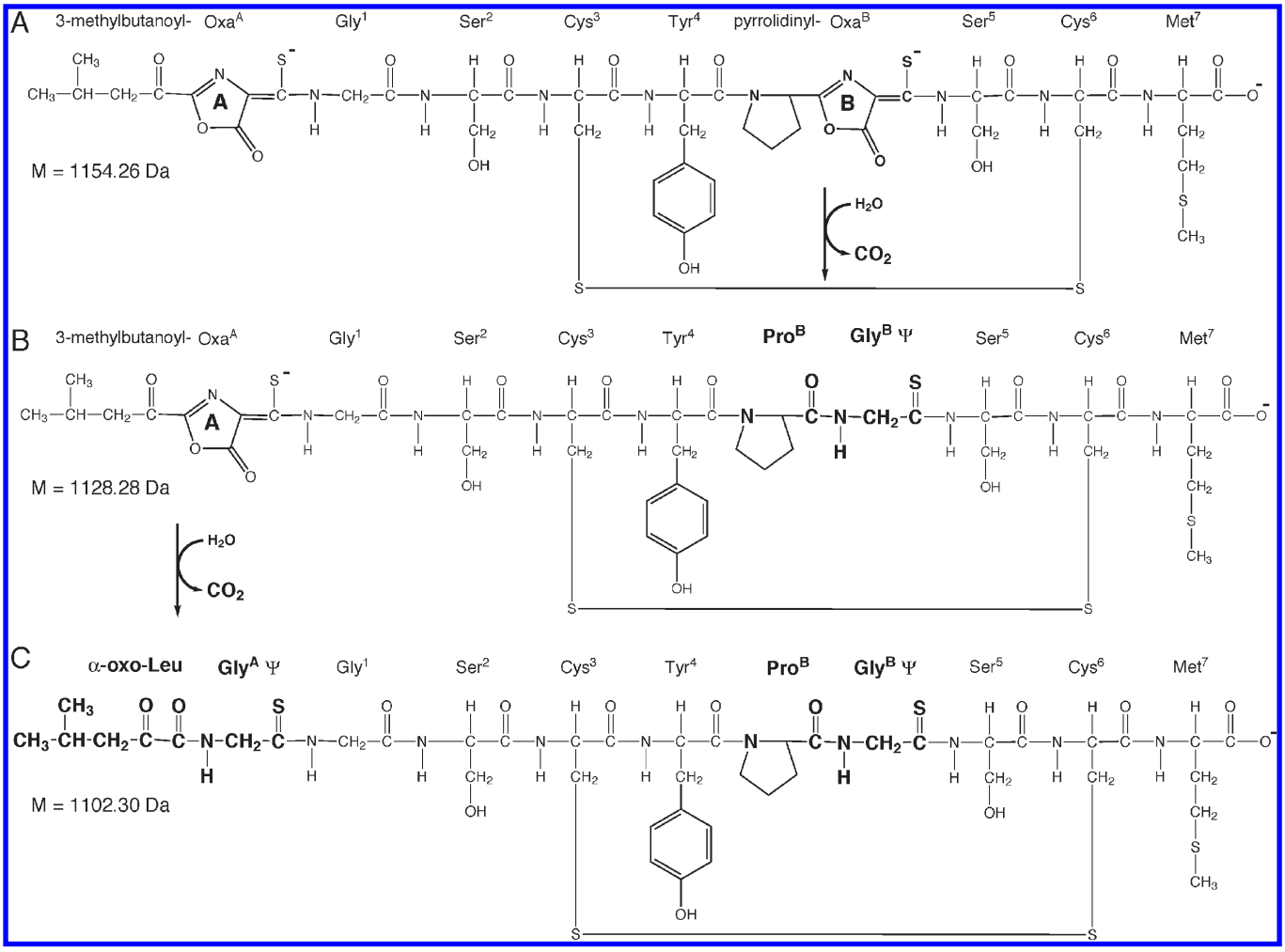

[a]The calculated exact mass for the neutral form of each structure is shown.

allowable start codon. This candidate mb-OB3b precursor gene is not identified as a coding region in the database record. This finding of a ribosomally produced precursor sequence for OB3b counters the suggestion made by others that mb-OB3b is produced nonribosomally (*14*).

Searching with the mb-OB3b precursor sequence against all nucleotide sequences in NCBI's nonredundant nucleic acid database identified one hit only, the 31-residue sequence MTIKIAKKQTLSVAGRAGACCGSCCAPVGVN from *Azospirillum* sp. B510. This sequence also was not previously annotated as a gene. The relatively high *E* value of the search result, 7.3, is an artifact of the shortness of the two sequences, because the level of sequence identity exceeds 50%. The level of sequence identity between the two precursors remains high in the leader peptide region that is absent from the mature form of mb-OB3b, suggesting a conserved mechanism of interaction with its maturation enzymes.

Examination of the neighboring genes shows that the putative methanobactin precursor genes belong to a set of six consecutive (i.e., five additional) genes for which the best match in any genome to the *M. trichosporium* OB3b protein occurs in *Azospirillum* sp. B510. Conversely, *Azospirillum* sp. B510 is an endophyte isolated from cultivated rice plants, where it inhabits the stem without causing disease (*19*). This α-Proteobacterium is diazotrophic (nitrogen-fixing) when free-living and appears to enhance both the growth rate and disease resistance in its plant host. The six loci in *Azospirillum* sp. B510 are AZL_007920, AZL_007930, the overlooked methanobactin precursor gene, AZL_007940, AZL_007950, and AZL_007960. For protein AZL_007930 from *Azospirillum* sp. B510, for instance, the best database match occurs in *M. trichosporium* OB3b and has an *E* value of 2×10^{-74}. No species other than *M. trichosporium* OB3b is represented among the top hits to more than two of these six genes. Furthermore, we were unable to identify additional homologues to the mb-OB3b precursor or the *Azospirillum* mb precursor in any other species. It appears, therefore, that this particular class of methanobactin, defined by conservation of both the precursor sequence and possible maturation enzymes, is relatively uncommon. Methanobactin biosynthesis systems are therefore likely to be quite diverse.

One of the conserved methanobactin precursor cluster genes (MettrDRAFT_3897 and its homologue AZL_007960) belongs to the multidrug and toxic compound extrusion (MATE) family (*20*) and is likely to participate in a transport process. Another member (MettrDRAFT_3900, AZL_007930) is a diheme enzyme related to CorB found in the methanotroph *Methylomicrobium album* BG8 (*21*), which is a copper-responsive homologue of bacterial diheme cytochrome *c* peroxidases, such as the surface-associated diheme cytochrome *c* peroxidase isolated from the methanotroph *Methylococcus capsulatutus* Bath (*22*). AZL_007930

and CorB are also homologous of MauG (methylamine utilization G), an enzyme that performs a tryptophan tryptophylquinone modification to the methylamine dehydrogenase small subunit (*23*).

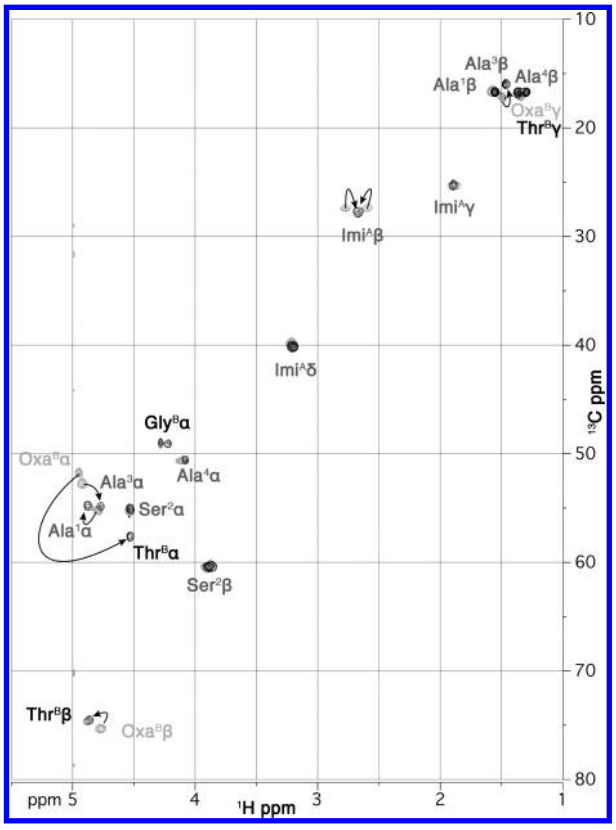

FIGURE 9: Overlay of the $^{1}H-^{13}C$ HSQC spectra before (gray) and after (black) the hydrolysis and decarboxylation of the oxazolone ring from SB2. Spectra were recorded in D_2O at 5 °C.

The adjacent gene (MettrDRAFT_3899, AZL_007920) appears to combine with the diheme enzyme to form a two-gene unit, as there are several additional species (e.g., *Myxococcus xanthus*) with tandem gene pairs closely related to AZL_007920 and AZL_007930. The two remaining genes in the region are AZL_007940 (split into two ORFs in *Methylosinus*), a member of the uncharacterized domain family DUF692, and MettrDRAFT_3896/AZL_007950, an uncharacterized protein with additional homologues only in the genus *Pseudomonas*. It is not clear at present which, if any, of the proteins in the cluster may act directly in methanobactin biosynthesis, cleavage, and transport and which might have other roles in copper metabolism.

DISCUSSION

Copper ions, while essential for all living cells, also present challenges. In their free form, Cu(II) ions catalyze Fenton-type reactions that produce destructive reactive oxygen species (ROS) (*24*). Living systems have therefore devised an array of strategies for acquiring and trafficking copper ions in ways that meet their copper requirements while at the same time protecting them from their damaging effects (*25*). Methanobactins are known to be important agents used by methanotrophic bacteria to acquire copper (*1*). With the chemical characterization of mb-SB2, there are now two defined methanobactin structures. Comparing these structures has allowed us to define the core features that they share and to appreciate the possible range of structures that can accommodate these core features.

Functionally, both mb-OB3b and mb-SB2 bind Cu(II) ions with high affinities and reduce them to Cu(I) (ref *13* and unpublished results of N. L. Bandow et al.). In addition, both methanobactins stabilize Cu(I) in an aqueous environment against disproportionation. In this report, we demonstrated that metal-free mb-OB3b and mb-SB2 are fragile molecules that readily degrade under mildly acidic conditions. However, once

Scheme 2: (A) Complete Primary Structure of mb-SB2 and (B) Product of Hydrolysis of the Oxazolone B-Ring in mb-SB2

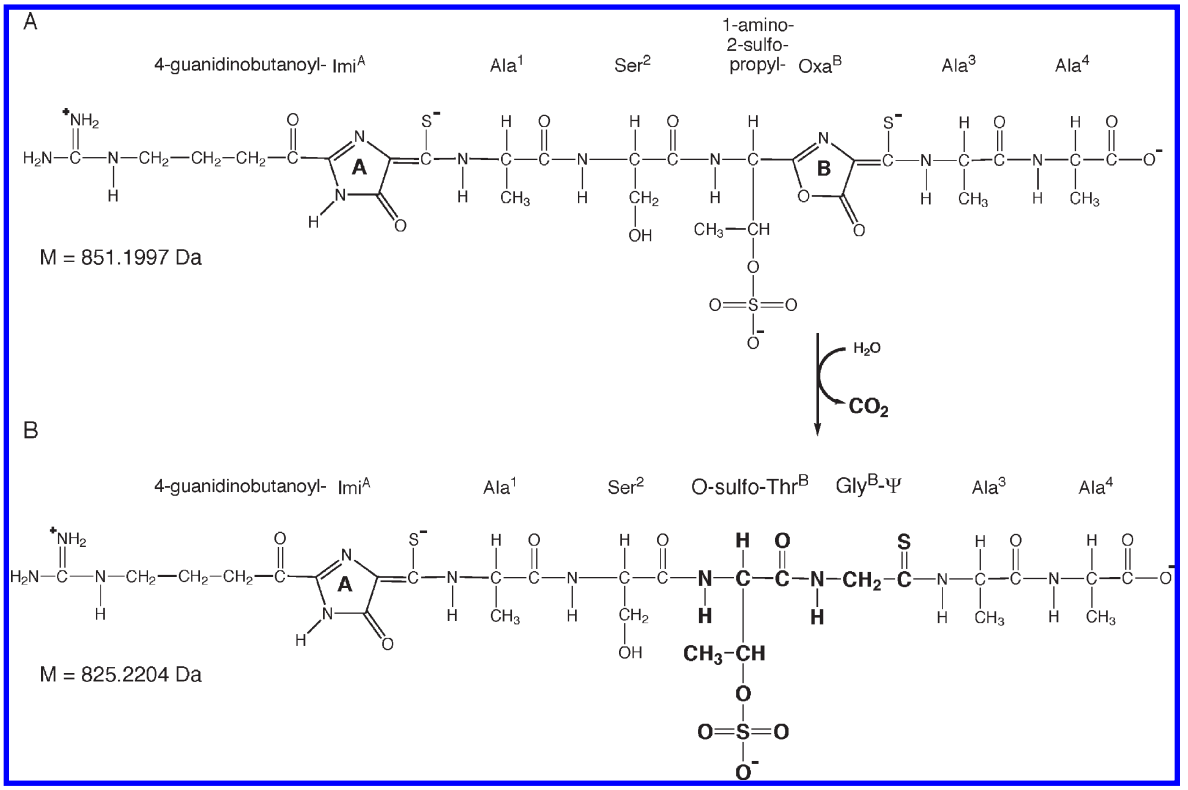

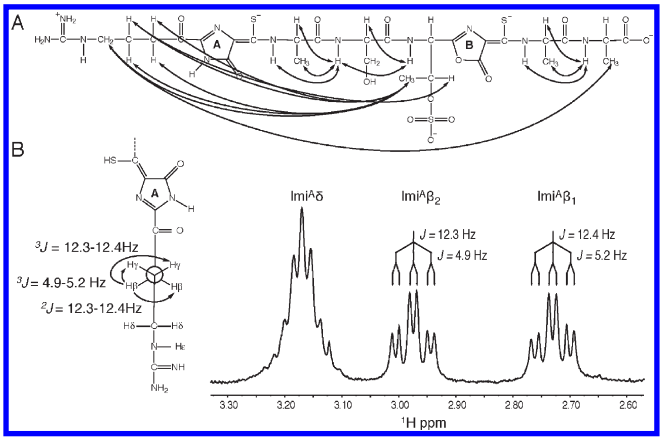

FIGURE 10: (A) Inter-residue dipolar couplings observed in ^{1}H−^{1}H ROESY experiments conducted on Cu(I)−mb-SB2 in both D_2O and a 90% H_2O/10% D_2O mixture at 25 °C. (B) Region of the ^{1}H spectrum for Cu(I)−mb-SB2 in a 90% H_2O/10% D_2O mixture at 25 °C showing the triplet-of-doublet splitting for both of the H^β atoms of the arginine-like side chain (4-guanidinobutanoyl group), which is associated with the A-ring imidazolone.

bound with Cu(I), both Cu(I)−mb-OB3b and Cu(I)−mb-SB2 are remarkably stable molecules.

A comparison of the two structures reveals that copper binding involves two five-member heterocyclic rings (see Figures 1 and 5). For mb-OB3b, both rings are oxazolones, and for mb-SB2, we find that the A-ring is instead an imidazolone. The imidazolone ring appears to provide the same required elements for effective Cu(I) binding as the oxazolone ring but is chemically more stable. For both mb-OB3b and mb-SB2, each ring is associated with an enethiol at the 4 position (Figures 1 and 5). For both molecules, the two enethiols contribute one sulfur atom each to the ligation of the Cu(I) ion. The crystal structure for mb-OB3b (*4*) shows that the N^3 atoms from each of the rings combine with the two enethiol sulfurs to form a distorted tetrahedral binding site for the Cu(I) ion. A crystal structure for mb-SB2 has not yet been determined; however, NMR evidence supports the formation of a similar binding site in mb-SB2. Figure 10A shows the inter-residue, dipolar couplings that are observed in a ^{1}H−^{1}H ROESY experiment. There are strong dipolar couplings between the protons of the arginine-like side chain (4-guanidinobutanoyl group in Figure 5) that is associated with the A-ring imidazolone, and the H^γ protons of the threonine-like side chain (1-amino-2-hydroxypropyl group in Figure 5) that is associated with the B-ring oxazolone. This indicates that the Cu(I)−mb-SB2 molecule is folded over into a hairpinlike structure that brings the two ring systems into the proximity of each other, presumably to bind the Cu(I) ion. Also, the ^{1}H spectrum for Cu(I)−mb-SB2 shows almost identical triplet-of-doublet splitting for each of the H^β atoms of the arginine-like side chain (Figure 10B). This splitting pattern indicates that this side chain is held very rigidly in the Cu(I)−mb-SB2 complex in an extended conformation that leads to equivalent sets of ^2J and ^3J couplings for the two H^β atoms. In addition, the narrowing of the enethiol peak in the S2p XPS spectrum upon Cu(I) binding (Figure 6) supports the involvement of the enethiol sulfurs in the formation of the copper binding site in mb-SB2.

A continuing mystery involving the interaction of methanobactins with Cu(II) is the source of the electron used to reduce the Cu(II) to Cu(I). With the exception of the loss of one proton per Cu(I) ion bound, the chemical composition of the methanobactin component of Cu(I)−mb-OB3b (*3*), and now Cu(I)−mb-SB2, appears to be unaltered by the reduction of Cu(II) to Cu(I). We have not identified the source of this electron, but there are several possibilities. The most obvious would be the thioamide/enethiol groups found in both mb-OB3b and mb-SB2. By analogy, thiourea has been shown to be an effective reductant of Cu(II) (*26*) and a ligand for Cu(I) complexes (*27*). However, the reduction is expected to produce a pair of disulfide-linked thiourea molecules as a product of a two-electron oxidation. This mechanism suggests that two populations of methanobactin should arise upon exposure to Cu(II), one that is responsible for reducing Cu(II) to Cu(I) and the other that binds and stabilizes Cu(I). However, we have so far seen no direct evidence supporting the formation of "sacrificial" methanobactin molecules containing newly formed disulfide bonds by LC−MS, NMR, or HPLC with UV−visible DAD detection. Some have suggested that the source of the electrons may be the sulfhydryl groups of the two cysteine residues found in mb-OB3b (*28*). However, this scenario predicts we should observe metal-free mb-OB3b molecules containing reduced cysteine sulfhydryl groups; however, we find that the disulfide is present, both in Cu(I)−mb-OB3b and in metal-free mb-OB3b, prior to the addition of Cu(II). Also, the absence of cysteine residues in mb-SB2 eliminates these amino acids as a possible electron source, at least for mb-SB2. A less likely option remains to be considered. Some type 1 copper sites in proteins, e.g., ceruloplasmin, are known to have extraordinarily high reduction potentials (> 1.0 V) (*29*, *30*). Such a high-potential site might be able to oxidize water, which has a reduction potential of ~0.8 V. Cu(I) prefers a tetrahedral ligand arrangement, while Cu(II) prefers a square planar, octahedral, or linear ligand arrangement. Forcing a Cu(II) ion into tetrahedral binding environment upon binding to methanobactins may give it a reduction potential much higher than expected. Given the remarkably high stability constant for the initial binding of Cu(II) by mb-OB3b ($\approx 10^{34}$, $\Delta G° \approx -194$ kJ/mol) (*13*), there is certainly free energy available to force such a distortion. The main experimental argument against this hypothesis is that we might expect to see hydroxyl radicals, peroxide, or even oxygen resulting from H_2O oxidation, and we so far have no evidence of the production of any of these products. Additional experiments conducted under completely dry conditions in DMSO, THF, or acetonitrile may help to answer this question.

The hydrolysis results obtained for both mb-OB3b and mb-SB2 demonstrate that hydrolysis targets the core regions that are involved in Cu(I) binding. The hydrolysis results also illustrate how UV−visible absorption can be used to monitor the state of the key contributors to these core regions. In addition to the absorbances at around 340 and 394 nm, which monitor the two heterocyclic rings, the UV−visible spectrum shows a single peak at 267 nm when both rings are removed from mb-OB3b (Figure 8C). This peak agrees with what others have reported for peptides containing thioamides (*17*); therefore, we assign this peak to the thioamide groups that form upon hydrolysis and decarboxylation of the oxazolone rings. mb-OB3b also contains a tyrosine residue, which has a phenolic group that will contribute to the absorbance at ~274 nm; however, the molar extinction coefficient for this group (1400 M^{-1}) is approximately one-sixth of that for the thioamide in this wavelength region (9000 M^{-1}) (*17*, *31*), so with two thioamide groups, the thioamide absorbance is expected to predominate. The UV−visible spectrum after only one of the two rings is removed from mb-OB3b shows an additional peak at 298 nm (Figure 8A), which can now be assigned to the remaining enethiol group. The UV−visible

Scheme 3: Proposed Pathway for the Biosynthesis of mb-OB3b

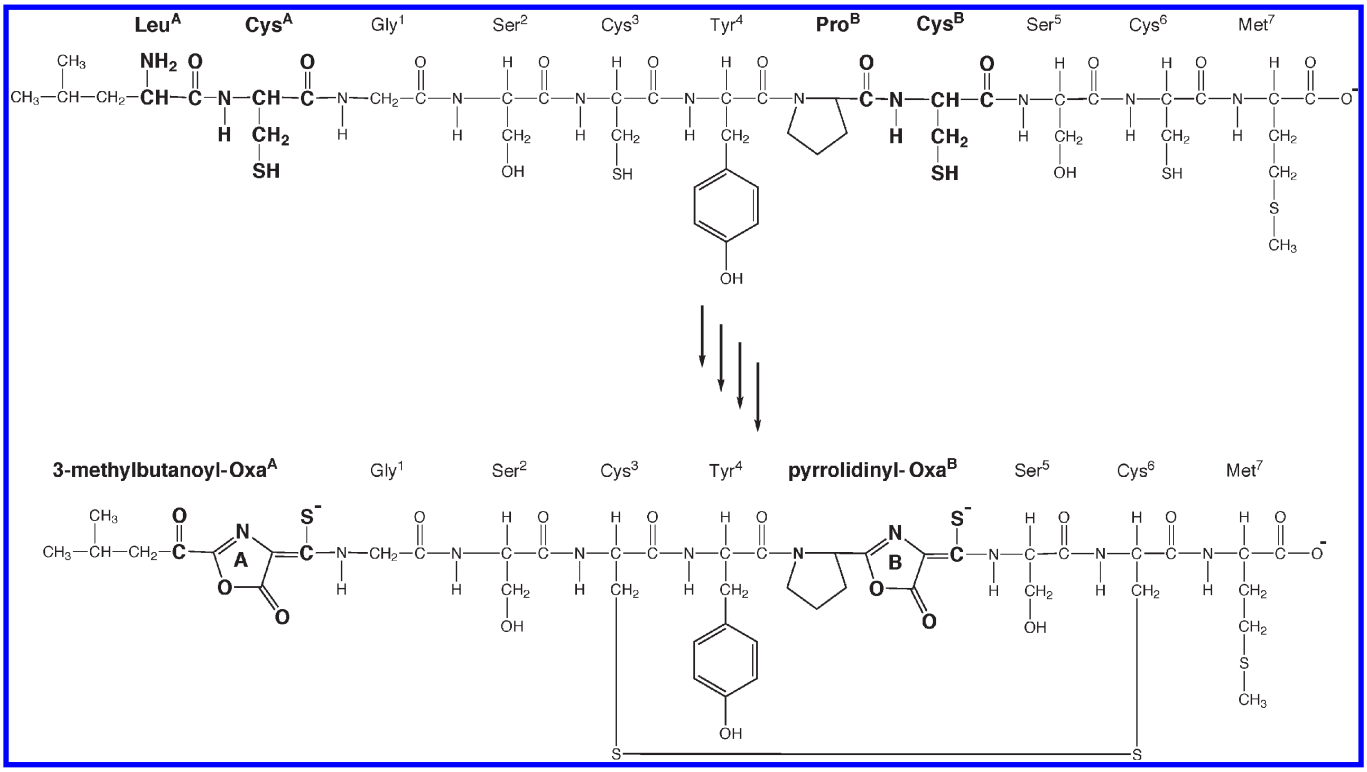

spectrum for mb-SB2 after removal of its single oxazolone ring (Figure 8E) looks nearly identical to that for mb-OB3b (compare to Figure 8A). Given the differences in structure between the two methanobactins, this again illustrates that UV−visible absorption conveniently monitors the state of the core features that are involved in Cu(I) binding, viz., the heterocyclic A- and B-rings along with their associated enethiols.

Aside from the core features that mb-OB3b and mb-SB2 share that are directly involved in Cu(I) binding, there are marked differences in the remaining portions of their chemical structures. Though both appear to be derived from a peptide, the choice of amino acids is quite different. In a previous report, we proposed that mb-OB3b is biosynthesized from an 11-residue peptide (*3*). Here we show that mb-OB3b can be converted back into an 11-residue peptide that contains only three minor modifications when compared to a standard peptide: the inclusion of two thioamides and the substitution of an α-oxo group for the N-terminal α-amino group: α-oxo-Leu-Gly-ψ-Gly-Ser-Cys-Tyr-Pro-Gly-ψ-Ser-Cys-Met-OH.

In the precursor peptide, the glycines are presumably substituted with amino acids having reactive side chains that can serve as starting points on a pathways leading to the formation of the oxazolone rings. Previously, we proposed serines (*3*); however, through analysis of the genomic data that are available for *M. trichosporium* OB3b, we now know that mb-OB3b is synthesized from a peptide precursor that places cysteines at these locations, LCGSCYPCSCM. With this sequence in hand, we now have both the starting and ending points for the pathway leading to the biosynthesis of mb-O3b3 (Scheme 3). Post-translational modifications of cysteines are known to form thiazole rings from ribosomally produced precursors of the thiopeptide antibiotics (*32*−*34*). Oxazolones would require a different set of post-translational modification; however, an appealing aspect for the involvement of a cysteine is that it could serve as the source for the sulfur used to make the adjacent thioamide. If the sulfur leaves by β-elimination as a sulfide, this could convert the cysteine to a dehydroalanine (*35*, *36*). Adding water across the double bond in the dehydroalanine could then lead to a serine that could go on to form an oxazolone by one of the pathways described previously (*3*). While this is still speculation, it is hoped that further analyses of the genes in the cluster associated with the mb-OB3b precursor may shed light on the detailed steps involved in the pathway.

Given the similarities in the copper-binding regions for mb-OB3b and mb-SB2, it is reasonable to propose that mb-SB2 is also synthesized in a similar way from a precursor peptide that has the following sequence: H_2N-Arg-Cys-Ala-Ser-Thr-Cys-Ala-Ala-OH

The formation of the imidazolone from the Arg-Cys dipeptide in mb-SB2 might involve a variation on the theme just described for oxazolone formation, where ammonia, instead of water, adds across the double bond in the proposed dehydroalanine and that this then proceeds to form the imidazolone in a manner homologous to that proposed for oxazolone formation. A possible source of the ammonia could be the deamination of the adjacent N-terminal α-amino group.

Though capable of forming a similar copper-binding core, the proposed mb-SB2 precursor sequence is significantly different from that for mb-OB3b and predicts that the primary structures for methanobactin precursor peptides may be quite diverse among methanotrophs. The sequence for the mb-SB2 precursor is substantially shorter, eight residues instead of 11, and replaces some of the potentially reactive amino acid side chains found in mb-OB3b (Cys, Tyr, and Met), with fairly nonreactive ones (Ala residues). Unlike mb-OB3b, mb-SB2 lacks an intramolecular disulfide bond. In mb-OB3b, the disulfide bond produces a 20-member ring (Figure 1). This ring should substantially reduce the conformational space for the mb-OB3b molecule and thereby increase the favorable negative free energy change for copper binding. mb-SB2 lacks a disulfide, but it has fewer intervening

residues between the two rings, which will also reduce its conformational space. It also has the sulfate group, which as we have shown is most likely attached to the threonine-like side chain of the intact molecule (Scheme 2A). This sulfate is expected to be situated near the tight turn that will be needed to bring the two halves of the binding site together and thereby may stabilize this turn by providing a number of hydrogen-bonding acceptor sites. Among the growing list of unusual structural features displayed by the methanobactins, the *O*-sulfothreonine for mb-SB2 should now be added. O-Sulfonation of serines and threonines in proteins and peptides has only rarely been observed in Nature. A small number of examples have been observed in eukaryotic systems (*37*), but mb-SB2 may represent the first example of a prokaryotic protein or peptide containing an *O*-sulfothreonine.

Finally, recent work has shown that two γ-Proteobacteria methanotrophs, *Me. capsulatus* Bath and *Met. album* BG8, also produce methanobactins, but preliminary structural characterization of these methanobactins shows them to be different from the two that have now been characterized for α-Proteobacteria methanotrophs (*8*). Furthermore, these methanobactins have substantially lower affinities for copper than mb-OB3b, as demonstrated by the ability of metal-free mb-OB3b to remove Cu(I) from the methanobactins produced by both γ-Proteobacterial methanotrophs. The acid labile nature of the methanobactins that we have characterized for *M. trichosporium* OB3b and *Methylocystis* strain SB2 could make these organisms poorly adapted to acquiring copper in acidic environments. It may be that the structural and chemical diversity of methanobactins made by methanotrophs helps to define the structural differences in the composition of methanotrophic communities in situ (*1*).

ACKNOWLEDGMENT

We thank David Lewis for his helpful chemical insights, James Harder for contributions to the hydrolysis experiments, and Emily Hoida and Nicholas Warren for contributions to the XPS analyses.

SUPPORTING INFORMATION AVAILABLE

Mass spectrum of metal-free mb-SB2 used to determine its exact mass, summaries of the ^{1}H, ^{13}C, and ^{15}N correlations used to deduce the chemical structure for mb-SB2, a table containing the ^{1}H, ^{13}C, and ^{15}N resonance assignments for Cu(I)−mb-SB2, and a table containing the ^{1}H and ^{13}C resonance assignments for metal-free mb-SB2, before and after hydrolysis and decarboxylation of its oxazolone ring. This material is available free of charge via the Internet at http://pubs.acs.org.

REFERENCES

1. Semrau, J. D., DiSpirito, A. A., and Yoon, S. (2010) Methanotrophs and copper. *FEMS Microbiol. Rev. 34*, 496–531.
2. Yoon, S., Kraemer, S. M., DiSpirito, A. A., and Semrau, J. D. (2010) An assay for screening microbial cultures for chalkophore production. *Environ. Microbiol. Rep. 2*, 295–303.
3. Behling, L. A., Hartsel, S. C., Lewis, D. E., DiSpirito, A. A., Choi, D. W., Masterson, L. R., Veglia, G., and Gallagher, W. H. (2008) NMR, mass spectrometry and chemical evidence reveal a different chemical structure for methanobactin that contains oxazolone rings. *J. Am. Chem. Soc. 130*, 12604–12605.
4. Kim, H. J., Graham, D. W., DiSpirito, A. A., Alterman, M. A., Galeva, N., Larive, C. K., Asunskis, D., and Sherwood, P. M. (2004) Methanobactin, a copper-acquisition compound from methane-oxidizing bacteria. *Science 305*, 1612–1615.
5. Im, J., Lee, S.-W., Yoon, S., DiSpirito, A., and Semrau, J. (2010) Characterization of a novel facultative *Methylocystis* species capable of growth on methane, acetate, and ethanol. *Environ. Microbiol. Rep.* DOI: 10.1111/j.1758-2229.2010.00204.x.
6. Martinho, M., Choi, D. W., DiSpirito, A. A., Antholine, W. E., Semrau, J. D., and Munck, E. (2007) Mossbauer studies of the membrane-associated methane monooxygenase from *Methylococcus capsulatus* Bath: Evidence for a diiron center. *J. Am. Chem. Soc. 129*, 15783–15785.
7. Yoon, S., Im, J., Bandow, N., DiSpirito, A., and Semrau, J. (2010) Constitutive expression of pMMO by *Methylocystis* strain SB2 when grown on multi-carbon substrates: Implications for biodegradation of chlorinated ethenes. *Environ. Microbiol. Rep.* DOI: 10.1111/j.1758-2229.2010.00205.x.
8. Choi, D. W., Bandow, N. L., McEllistrem, M. T., Semrau, J. D., Antholine, W. E., Hartsel, S. C., Gallagher, W., Zea, C. J., Pohl, N. L., Zahn, J. A., and DiSpirito, A. A. (2010) Spectral and thermodynamic properties of methanobactin from γ-proteobacterial methane oxidizing bacteria: A case for copper competition on a molecular level. *J. Inorg. Biochem. 104*, 1240–1247.
9. Whittenbury, R., Phillips, K. C., and Wilkinson, J. F. (1970) Enrichment, isolation and some properties of methane-utilizing bacteria. *J. Gen. Microbiol. 61*, 205–218.
10. Choi, D. W., Do, Y. S., Zea, C. J., McEllistrem, M. T., Lee, S. W., Semrau, J. D., Pohl, N. L., Kisting, C. J., Scardino, L. L., Hartsel, S. C., Boyd, E. S., Geesey, G. G., Riedel, T. P., Shafe, P. H., Kranski, K. A., Tritsch, J. R., Antholine, W. E., and DiSpirito, A. A. (2006) Spectral and thermodynamic properties of Ag(I), Au(III), Cd(II), Co(II), Fe(III), Hg(II), Mn(II), Ni(II), Pb(II), U(IV), and Zn(II) binding by methanobactin from *Methylosinus trichosporium* OB3b. *J. Inorg. Biochem. 100*, 2150–2161.
11. Altschul, S. F., Madden, T. L., Schaffer, A. A., Zhang, J., Zhang, Z., Miller, W., and Lipman, D. J. (1997) Gapped BLAST and PSI-BLAST: A new generation of protein database search programs. *Nucleic Acids Res. 25*, 3389–3402.
12. Edgar, R. C. (2004) MUSCLE: A multiple sequence alignment method with reduced time and space complexity. *BMC Bioinf. 5*, 113.
13. Choi, D. W., Zea, C. J., Do, Y. S., Semrau, J. D., Antholine, W. E., Hargrove, M. S., Pohl, N. L., Boyd, E. S., Geesey, G. G., Hartsel, S. C., Shafe, P. H., McEllistrem, M. T., Kisting, C. J., Campbell, D., Rao, V., de la Mora, A. M., and DiSpirito, A. A. (2006) Spectral, kinetic, and thermodynamic properties of Cu(I) and Cu(II) binding by methanobactin from *Methylosinus trichosporium* OB3b. *Biochemistry 45*, 1442–1453.
14. Kim, H. J., Galeva, N., Larive, C. K., Alterman, M., and Graham, D. W. (2005) Purification and physical-chemical properties of methanobactin: A chalkophore from *Methylosinus trichosporium* OB3b. *Biochemistry 44*, 5140–5148.
15. Choi, D. W., Antholine, W. E., Do, Y. S., Semrau, J. D., Kisting, C. J., Kunz, R. C., Campbell, D., Rao, V., Hartsel, S. C., and DiSpirito, A. A. (2005) Effect of methanobactin on the activity and electron paramagnetic resonance spectra of the membrane-associated methane monooxygenase in *Methylococcus capsulatus* Bath. *Microbiology* (*Reading, U.K.*) *151*, 3417–3426.
16. Wagner, C. D., Naumkin, A. V., Kraut-Vass, A., Allison, J. W., Powell, C. J., Rumble, J., and John, R. (2003) NIST X-ray Photoelectron Spectroscopy Database, National Institute of Standards and Technology, Gaithersburg, MD.
17. Zhao, J., Wildemann, D., Jakob, M., Vargas, C., and Schiene-Fischer, C. (2003) Direct photomodulation of peptide backbone conformations. *Chem. Commun.*, 2810–2811.
18. Jaeger, E., Remmer, H. A., Jung, G., Metzger, J., Oberthur, W., Rucknagel, K. P., Schafer, W., Sonnenbichler, J., and Zetl, I. (1993) Side-reactions in peptide-synthesis. 5. O-Sulfonation of serine and threonine during removal of the PMC-protecting and MTR-protecting groups from arginine residues in FMOC-solid-phase synthesis. *Biol. Chem. Hoppe-Seyler 374*, 349–362.
19. Kaneko, T., Minamisawa, K., Isawa, T., Nakatsukasa, H., Mitsui, H., Kawaharada, Y., Nakamura, Y., Watanabe, A., Kawashima, K., Ono, A., Shimizu, Y., Takahashi, C., Minami, C., Fujishiro, T., Kohara, M., Katoh, M., Nakazaki, N., Nakayama, S., Yamada, M., Tabata, S., and Sato, S. (2010) Complete genomic structure of the cultivated rice endophyte *Azospirillum* sp. B510. *DNA Res. 17*, 37–50.
20. Kuroda, T., and Tsuchiya, T. (2009) Multidrug efflux transporters in the MATE family. *Biochim. Biophys. Acta 1794*, 763–768.
21. Karlsen, O. A., Larsen, O., and Jensen, H. B. (2010) Identification of a bacterial di-heme cytochrome c peroxidase from *Methylomicrobium album* BG8. *Microbiology* (*Reading, U.K.*) *156*, 2682–2690.

22. Karlsen, O. A., Kindingstad, L., Angelskar, S. M., Bruseth, L. J., Straume, D., Puntervoll, P., Fjellbirkeland, A., Lillehaug, J. R., and Jensen, H. B. (2005) Identification of a copper-repressible C-type heme protein of *Methylococcus capsulatus* (Bath). A member of a novel group of the bacterial di-heme cytochrome c peroxidase family of proteins. *FEBS J. 272*, 6324–6335.
23. Wang, Y., Li, X., Jones, L. H., Pearson, A. R., Wilmot, C. M., and Davidson, V. L. (2005) MauG-dependent in vitro biosynthesis of tryptophan tryptophylquinone in methylamine dehydrogenase. *J. Am. Chem. Soc. 127*, 8258–8259.
24. Kremer, M. L. (2006) Promotion of the Fenton reaction by Cu^{2+} ions: Evidence for intermediates. *Int. J. Chem. Kinet. 38*, 725–736.
25. Boal, A. K., and Rosenzweig, A. C. (2009) Structural biology of copper trafficking. *Chem. Rev. 109*, 4760–4779.
26. Kratochvil, B., Zatko, D. A., and Markuszewski, R. (1966) Copper-(II) as an analytical oxidant in acetonitrile. *Anal. Chem. 38*, 770–772.
27. Zhu, B.-Z., Antholine, W. E., and Frei, B. (2002) Thiourea protects against copper-induced oxidative damage by formation of a redox-inactive thiourea-copper complex. *Free Radical Biol. Med. 32*, 1333–1338.
28. Hakemian, A. S., Tinberg, C. E., Kondapalli, K. C., Telser, J., Hoffman, B. M., Stemmler, T. L., and Rosenzweig, A. C. (2005) The copper chelator methanobactin from *Methylosinus trichosporium* OB3b binds copper(I). *J. Am. Chem. Soc. 127*, 17142–17143.
29. Machonkin, T. E., Zhang, H. H., Hedman, B., Hodgson, K. O., and Solomon, E. I. (1998) Spectroscopic and magnetic studies of human ceruloplasmin: Identification of a redox-inactive reduced type 1 copper site. *Biochemistry 37*, 9570–9578.
30. Li, H., Webb, S. P., Ivanic, J., and Jensen, J. H. (2004) Determinants of the Relative Reduction Potentials of Type-1 Copper Sites in Proteins. *J. Am. Chem. Soc. 126*, 8010–8019.
31. Fasman, G. D. (1976) Handbook of Biochemistry and Molecular Biology, Proteins, 3rd ed., Vol. I, CRC Press, Boca Raton, FL.
32. Li, Y. M., Milne, J. C., Madison, L. L., Kolter, R., and Walsh, C. T. (1996) From peptide precursors to oxazole and thiazole-containing peptide antibiotics: Microcin B17 synthase. *Science 274*, 1188–1193.
33. Nolan, E. M., and Walsh, C. T. (2009) How nature morphs peptide scaffolds into antibiotics. *ChemBioChem 10*, 34–53.
34. Arndt, H.-D., Schoof, S., and Lu, J.-Y. (2009) Thiopeptide Antibiotic Biosynthesis. *Angew. Chem., Int. Ed. 48*, 6770–6773.
35. Sokolovsky, M., Sadeh, T., and Patchornik, A. (1964) Nonenzymic cleavages of peptide chains at the cysteine and serine residues through their conversion into dehydroalanine. II. Specific chemical cleavage of cysteinyl peptides. *J. Am. Chem. Soc. 86*, 1212–1217.
36. Bernardes Goncalo, J. L., Chalker Justin, M., Errey James, C., and Davis Benjamin, G. (2008) Facile conversion of cysteine and alkyl cysteines to dehydroalanine on protein surfaces: Versatile and switchable access to functionalized proteins. *J. Am. Chem. Soc. 130*, 5052–5053.
37. Medzihradszky, K. F., Darula, Z., Perlson, E., Fainzilber, M., Chalkley, R. J., Ball, H., Greenbaum, D., Bogyo, M., Tyson, D. R., Bradshaw, R. A., and Burlingame, A. L. (2004) O-Sulfonation of serine and threonine: Mass spectrometric detection and characterization of a new posttranslational modification in diverse proteins throughout the eukaryotes. *Mol. Cell. Proteomics 3*, 429–440.